Monthly Notices of the ROYAL ASTRONOMICAL SOCIETY
MNRAS **526,** 2251–2264 (2023) https://doi.org/10.1093/mnras/stad2822
Advance Access publication 2023 September 18

Exploring the potential of *Twinkle* to unveil the nature of LTT 1445 Ab

Caprice L. Phillips,[1★] Ji Wang (王吉),[1] Billy Edwards,[2] Romy Rodríguez Martínez,[1] Anusha Pai Asnodkar[1] and B. Scott Gaudi[1]

[1] *Department of Astronomy, The Ohio State University, Columbus, OH 43210, USA*
[2] *SRON, Netherlands Institute for Space Research, Niels Bohrweg 4, NL-2333 CA, Leiden, the Netherlands*

Accepted 2023 September 11. Received 2023 September 8; in original form 2022 September 27

ABSTRACT

We explore the prospects for *Twinkle* to determine the atmospheric composition of the nearby terrestrial-like planet LTT 1445 Ab, including the possibility of detecting the potential biosignature ammonia (NH_3). At a distance of 6.9 pc, this system is the second closest known transiting system and will be observed through transmission spectroscopy with the upcoming *Twinkle* mission. Although LTT 1445 Ab has been suggested to be a candidate for a Hycean world, constraints on the interior composition based on its mass and radius suggests that the planet lacks a substantial water layer, and thus the proposed Hycean scenario is disfavoured. We use PETITRADTRANS and a *Twinkle* simulator to simulate transmission spectra for the more likely scenario of a cold Haber world for which NH_3 is considered to be a biosignature. We study the detectability under different scenarios: varying hydrogen fraction, concentration of ammonia, and cloud coverage. We find that ammonia can be detected at an $\sim 3\sigma$ level for optimal (non-cloudy) conditions with 25 transits and a volume mixing ration of 4.0 ppm of NH_3. We provide examples of retrieval analysis to constrain potential NH_3 and H_2O in the atmosphere. Our study illustrates the potential of *Twinkle* to characterize atmospheres of potentially habitable exoplanets.

Key words: astrobiology – telescopes – planets and satellites: atmospheres – planets and satellites: terrestrial planets.

1 INTRODUCTION

Twinkle is an upcoming space-based telescope with a 0.45 m primary aperture and a broad visible to infrared wavelength coverage (0.5–4.5 µm). The *Twinkle* space mission (Stotesbury et al. 2022) will conduct two simultaneous surveys during its first three years of operation, which is scheduled to begin in 2025. While one of these will focus on studying objects within our Solar system, the other will be dedicated to the study of extrasolar targets. A large portion of the latter survey will be used to study exoplanet atmospheres, the science case for which *Twinkle* was originally conceived (Edwards et al. 2019). There are nearly 900 confirmed transiting exoplanets within *Twinkle's* field of view, as well as over 1400 planet candidates from the *Transiting Exoplanet Survey Satellite* (*TESS*, Ricker et al. 2015), offering the potential for a structured population survey of exoplanet atmospheres.

Twinkle can be highly complementary to *JWST*. While *JWST* will deliver unprecedentedly precise data, there will be limited time allocated to exoplanet sciences. Therefore, it is likely to only be used to observe the most exciting targets. To this end, *Twinkle* can provide low-resolution spectroscopy to provide an initial atmospheric characterization to promote further study or be used to refine planetary and orbital parameters. Moreover, certain *JWST* instruments/modes cannot observe bright targets due to saturation limits, and *Twinkle* can fill in the gap for bright targets. Furthermore, the planets studied with *Twinkle* can be methodically selected, building up large sets of data with specific goals in mind whereas each *JWST* proposal often focuses only on a small number of worlds. Combining *Twinkle* data with the *JWST* mission will allow us to achieve a more comprehensive picture of exoplanet atmospheres.

Current ground-based atmospheric characterization of super-Earth/terrestrial planets have proven difficult due to challenges such as photon noise limits, wavelength coverage, and telluric contamination. Photon noise can be improved by extremely large telescopes such as Giant Magellan Telescope and European Extremely Large Telescope. Current and future space-based facilities can address the wavelength coverage and telluric contamination issues.

The Kepler Space Mission (Borucki et al. 2010) has shown that super-Earths/mini-Neptunes are among the most abundant type of planet (Fressin et al. 2013; Fulton et al. 2017). There is an observed gap in the distribution of these planet sizes, known as the radius valley (Fulton et al. 2017; Van Eylen et al. 2018). Below the radius valley ($<1.5\,R_\oplus$), these planets are known as super-Earths/terrestrial-like planets. Studies have investigated their ability to hold onto a hydrogen-based atmosphere due to their decreased mass and decreased surface gravity from both ground-based (Diamond-Lowe et al. 2018, 2020, 2022) and space-based observatories (de Wit et al. 2016; Edwards et al. 2021; Garcia et al. 2022).

Planets with H_2/He dominated atmospheres may be more amenable targets for transmission spectroscopy with upcoming space-based missions such as *Twinkle*. The presence of H_2 can raise the scale height and therefore the transmission signal features for observations (Miller-Ricci, Seager & Sasselov 2008; Hu et al. 2021). H_2-dominated atmospheres may also produce different biosignatures, such as NH_3 in cold Haber worlds (see Section 2;

★ E-mail: phillips.1622@buckeyemail.osu.edu

Seager, Bains & Hu 2013a). Habitability and biosignature prospects have been explored in ocean/water and Hycean worlds (e.g. Léger et al. 2004; Selsis et al. 2007; Zeng & Sasselov 2014; Thomas & Madhusudhan 2016; Noack, Snellen & Rauer 2017; Ramirez & Levi 2018). Hycean worlds (Madhusudhan, Piette & Constantinou 2021) are planets with potentially habitable large oceans underneath a H_2-rich atmosphere. Dominant biomarkers proposed in Hycean atmospheres are dimethylsulfide, CS_2, CH_3Cl, OCS, and N_2O (Madhusudhan et al. 2021)

In this work, we assess the detectability of the potential biosignature ammonia on the terrestrial-like planet, LTT 1445 Ab, with the upcoming *Twinkle* space mission. We first provide a summary of previous literature on ammonia as a potential biosignature in Section 2. We then describe the target selection process that leads to the focus on the study of LTT 1445 Ab in Section 3. The process to distinguish LTT 1445 Ab from a cold Haber world or Hycean world is described in Section 4. Major findings on the detectability of NH_3 are presented in Section 5. Finally, we present our retrieval analysis to support the major findings in Section 6 and conclude in Section 7.

2 AMMONIA AS A POTENTIAL BIOSIGNATURE

A biosignature is nominally defined as an ‘object, substance, and/or pattern whose origin specifically requires a biological agent’ (Des Marais et al. 2002, 2008). Ideal and useful biosignatures gas have the following properties: they can accumulate in the atmosphere, are spectroscopically active, and not overly contaminated by geophysical false positives (Meadows & Seager 2010).

Seager et al. (2013a) proposed NH_3 as a biosignature gas in an H_2 and N_2 dominated atmosphere – nicknamed a cold Haber world (e.g. Seager, Bains & Hu 2013b; Huang et al. 2021). Cold Haber worlds are named after the Haber–Bosch process which is the main industrial process for producing NH_3 from N_2 from the air, H_2 from natural gas, and a metal catalyst, combined under high temperatures and pressures. The reaction is as follows:

$$3H_2 + N_2 \longrightarrow 2NH_3.$$

In a H_2–N_2 environment life would have a metabolic enticement for the high production of NH_3 (Seager et al. 2013a; Ranjan et al. 2022). NH_3 in a terrestrial planet atmosphere is generally a good biosignature gas, primarily because terrestrial planets have no significant known abiotic NH_3 source (Huang et al. 2021).

Although NH_3 is a strong candidate biosignature in H_2 and N_2 atmospheres, there is still need to consider the potential of false positives. Some of these false positives include inorganic ammonia ice brought from comet collisions, outgassed NH_3, NH_3 produced on an iron surface of a planet (surface temperature ~ 820 K),[1] and natural NH_3 present in mini-Neptunes. An overview of false positives of NH_3 was provided by Seager et al. (2013b) and Catling et al. (2018), alongside thesis work by Evan Sneed.[2] Recently, Huang et al. (2021) laid out a few examples of minor abiotic sources of NH_3 for Earth/terrestrial-like planets including: trace components in volcanic gas eruptions, iron doping TiO_2 containing sands, and lightning.

Since the proposal of NH_3 as a biosignature, there have been a multitude of studies to investigate its detectability with *JWST* and future Extremely Large Telescopes (e.g. Chouqar et al. 2020; Wunderlich et al. 2020; Phillips et al. 2021; Ranjan et al. 2022). Phillips et al. (2021) explored the detection of the potential biosignature NH_3 in gas dwarfs, exoplanets with radii between Earth and Neptune with potentially H_2 dominated atmospheres. They found that a minimum of 0.4 ppm would be needed to detect the ammonia features in transmission spectroscopy with the Near-Infrared Spectrograph (NIRSpec) and Near Infrared Imager and Slitless Spectrograph (NIRISS) (SOSS) instruments/modes on *JWST*, given optimal cloud-free atmospheric conditions. Huang et al. (2021) assessed ammonia as a potential biosignature in terrestrial planets with H_2-dominated atmospheres and found that a minimum of 5.0 ppm ammonia in the atmosphere would be needed to be detectable by *JWST* using the NIRSpec/G395M mode for the 3.0 μm ammonia feature. In this work, we aim to perform similar studies for the detectability of NH_3 with *Twinkle* and quantify necessary conditions for detection.

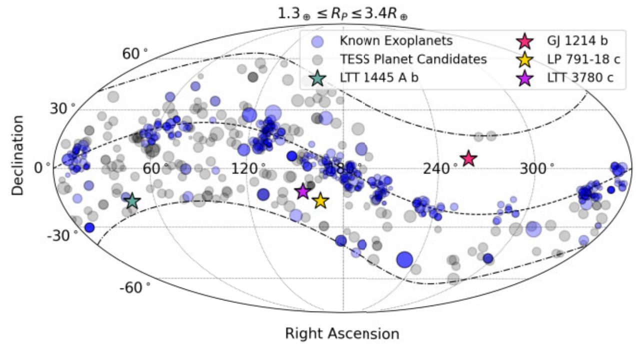

Figure 1. Field of view showing known exoplanets (blue circles) with planetary size ($1.3_\oplus \leq R_p \leq 3.4_\oplus$). The *TESS* planet candidates are shown in the grey markers. The size of the markers correspond to the host star's *K*-band magnitude. The target of interest for this paper LTT 1445 Ab is shown with a star marker. Labelled planet GJ 1214 b, LP 791-18 c, and LTT 3780 c, are shown with a pink, gold, and purple star, respectively.

3 TARGET SELECTION

We explore possible targets of interest for characterization that are within the field of view for *Twinkle* (Fig. 1). Targets are evaluated using the following criteria: (1) planet radii between 1.3 and 3.4 $R_\oplus$, (2) equilibrium temperature (T_{eq}) below 650 K, (3) distance within 50 pc, (4) an initial S/N estimation ($\langle S/N \rangle \geq 3\sigma$) for *Twinkle* using TWINKLERAD (Edwards & Stotesbury 2021) for a baseline of 25 transits, and (5) a modified transmission spectroscopy metric (TSM) from Kempton et al. (2018) (see equation 1).

Compared to the work in Phillips et al. (2021), we use an expanded parameter space of radii and equilibrium temperatures for our target selection. Nixon & Madhusudhan (2021) found that the phase structure of water-rich sub-Neptunes show indication that planets with a H/He envelope could host liquid H_2O in the liquid phase at up to 647 K at pressures of 218–7 $\times$ 10^4 bar. We also explore a slightly lower radius space (1.3 $R_\oplus$), as Huang et al. (2021) evaluated ammonia as a promising biosignature on terrestrial-like planets (e.g. a 1.75 and 10 $M_\oplus$ exoplanet around an M-dwarf). The distance criterium for objects within 50 pc is set to ensure sufficient flux for observations for the host star and planet

[1] At high surface temperatures, ammonia can be produced by the traditional Haber process from an iron surface.

[2] https://scholarsphere.psu.edu/resources/6c6f6ce8-3a94-40f5-a895-4165556b0f58

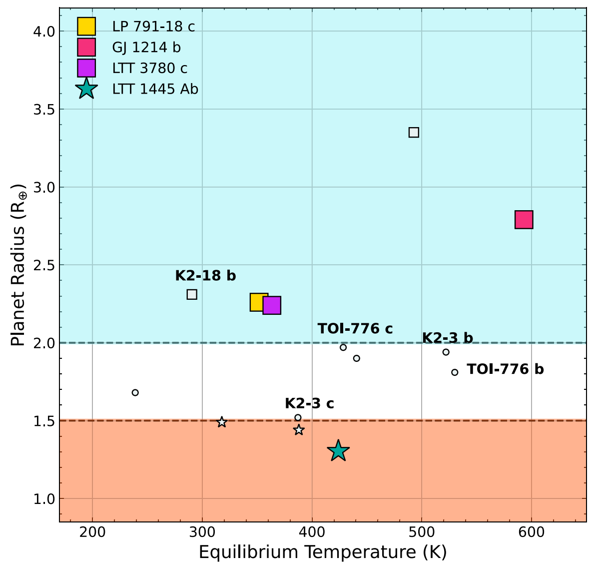

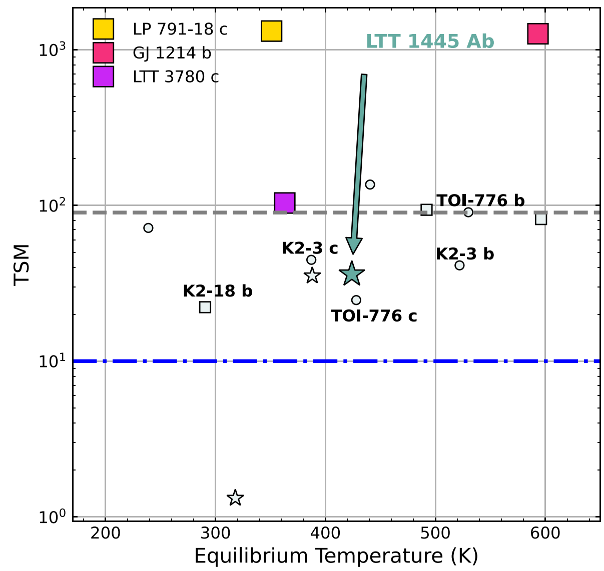

Figure 2. *Left:* Planet radius ($R_{\oplus}$) versus equilibrium temperature (K) for *Twinkle* objects that meet initial selection criteria (1–3). The orange shaded region and star shapes are objects below the radius valley ($<1.5\,R_{\oplus}$). Objects within the radius valley (1.5–2.0 $R_{\oplus}$) are marked with circle shapes. The blue shaded regions and square markers are targets above the radius valley ($>2.0\,R_{\oplus}$). The target of interest for this study LTT 1445 Ab is marked with a blue–green star. Other labelled planets are Hycean candidates that meet our initial selection criteria. *Right:* The modified transmission spectroscopy metric (TSM) for *H* band defined by Kempton et al. (2018). There are larger planets above the radius valley with the highest TSM: GJ 1214 b (pink square), LTT 3780 c (purple square), and LP 791-18 c (gold square). However, these targets have low S/N estimates with *Twinkle* for 25 transits or flat transmission spectra. The horizontal grey line represents the recommended TSM threshold for targets ($R = 1.5$–$10.0\,R_{\oplus}$) to be considered to be selected for high quality atmospheric characterization (Kempton et al. 2018). The blue dotted–dashed line represents the threshold TSM values (TSM > 10) for terrestrial like planets ($<1.5\,R_{\oplus}$).

We search the NASA Exoplanet Archive[3] for targets that meet our criteria. We find that LTT 1445 Ab has the highest (modified) TSM for terrestrial targets below the radius valley (Fig. 2). We also explore targets that lie within the radius valley, but find low S/N estimates for NH_3 detection given the baseline of 25 transits (Table 1). Initially objects such as GJ 1214 b, LP 791-18 c, and LTT 3780 c meet the first three criteria for target selection and produce high TSM metrics for planets above the radius valley. However, these targets either have known flat transmission spectra (Kreidberg et al. 2014) and/or currently have low S/N estimates for *Twinkle*. Therefore, we focus on LTT 1445 Ab in subsequent analyses.

3.1 LTT 1445 Ab

Since LTT 1445 Ab is a potential target, we provide a brief introduction of the system. LTT 1445 Ab lies at a distance of 0.038 AU from its host star and has an orbital period of 5.4 d (Winters et al. 2019). The host system is comprised of three mid-to-late M dwarfs. The host star, LTT 1445 A, is bright ($K_s = 6.50$ mag). LTT 1445 A is also the closest M-dwarf to host a transiting planet (Winters et al. 2021), making this system a prime target for atmospheric characterization. A summary of key stellar and planetary parameters is shown in Table 2. During the first three years of operations, *Twinkle* will conduct an extrasolar survey (Stotesbury et al. 2022). We use the tool from Edwards & Stotesbury (2021) to determine that, during the time frame of this survey, there will be 29 transits available for observation with *Twinkle*.

Despite the relative small size of LTT 1445 Ab, it is a target of interest for atmospheric studies. Winters et al. (2021) calculate a TSM of 30 for LTT 1445 Ab which is higher than those for LHS 1140 b (Dittmann et al. 2017) and TRAPPIST 1-f (Gillon et al. 2017). We implement a modified version of the Kempton TSM (equation 1),

$$\mathrm{TSM} = (\text{Scale factor}) \times \frac{R_p^3 T_{eq}}{M_p R_\star^2} \times 10^{-m_x/5}. \quad (1)$$

In equation (1), T_{eq} is the planet equilibrium temperature in Kelvin, R_p is the planet radius is Earth radii, M_p is the planet mass in Earth mass, $R_\star$ is the host star radius in solar radii, and m_x is the apparent magnitude of the host star.

The scale factor in equation (1) is designed to be a normalization constant to give near-realistic S/N values for 10 h observing with the *JWST*/NIRISS instrument (Kempton et al. 2018). The scale factor is different for planets with $R < 1.5\,R_{\oplus}$ (scale factor $= 0.190$) and planets with $1.5\,R_{\oplus} < R < 2.75\,R_{\oplus}$ (scale factor $= 1.26$). For more details about the method used and scale factor determination, see Kempton et al. (2018).

We evaluate the TSM using the *H*-band and *L*-band magnitude of LTT 1445 Ab. The *H* band has approximately the same central wavelength as the Channel 0 spectroscopic channel of Twinkle, which covers 0.5–2.4 microns, whereas the *L* band has approximately same wavelength as Channel 1, which covers 2.4–4.5 microns. We find an *H* -band TSM of 36.0 (Fig. 2) and *L*-band TSM of 44.0.

4 A HABER WORLD VERSUS A HYCEAN WORLD

In this section, we explore the scenario of LTT 1445 Ab as a Hycean world (Madhusudhan et al. 2021) and the implications for characterizing its atmosphere with *Twinkle*. A Hycean world is defined as a planet that has a water-rich interior with massive oceans underneath a H_2-dominated atmosphere (Madhusudhan et al. 2021).

[3] https://exoplanetarchive.ipac.caltech.edu/

Table 1. Twinkle targets of interest that meet our selection criteria 1–3. Additional criteria for the Total <S/N> and TSM *H* band are provided for targets of interest.

Name	R_p ($R_\oplus$)	T_{eq} (K)	Distance (pc)	Total <S/N> [a]	TSM (*H* band)[b]
GJ 1214 b	2.79	593.1	14.64	3.77	1265.67
LTT 1445 Ab[c]	1.30	424.0	14.90	3.10	36.0
TOI-776 b[c]	1.81	530.05	27.17	1.39	24.67
TOI-776 c[c]	1.97	428.43	27.17	1.16	90.41
G9-40 b	1.90	440.6	27.80	0.92	136.16
HD 3167 c	2.79	596.1	47.28	0.90	81.73
K2-3 b[c]	1.94	501.3	44.00	0.86	41.22
LTT 3780 c	2.24	363.41	21.98	0.82	103.64
TOI-237 b	1.44	388.0	38.11	0.79	35.35
LP 791-18 c	2.26	351.77	26.49	0.78	1316.86
LHS 1140 b	1.68	238.91	14.98	0.72	71.70
K2-3 c[c]	1.50	371.8	44.0	0.66	44.74
K2-25 b	3.35	492.77	44.95	0.33	93.75
K2-18 b[c]	2.30	290.8	38.00	0.30	22.2

[a]Total <S/N> is the the quadrature sum of the four NH_3 features at 1.5, 2.0, 2.3, and 3.0 μm. [b]TSM (*H* band) is modified TSM metric for Twinkle in equation (1). [c]Hycean candidates (Madhusudhan et al. 2021) that meet our initial selection criteria and are within Twinkle's field of view.

Table 2. Planetary and stellar parameters for LTT 1445 Ab from Winters et al. (2021).

M_p ($M_\oplus$)	$2.87^{+0.26}_{-0.25}$
R_p ($R_\oplus$)	$1.304^{+0.067}_{-0.060}$
T_{eq}(K)	424 ± 21
Distance (pc)	14.98 ± 0.01
H-band$_s$ (mag)	6.774 ± 0.038
T_s (K)	3337 ± 150
logg (dex)	$3.217^{+0.050}_{-0.053}$
t_{14} (h)	$1.367^{+0.017}_{-0.016}$
Fe/H (dex)	-0.34 ± 0.08
Eccentricity	$0.19^{+0.35}_{-0.14}$

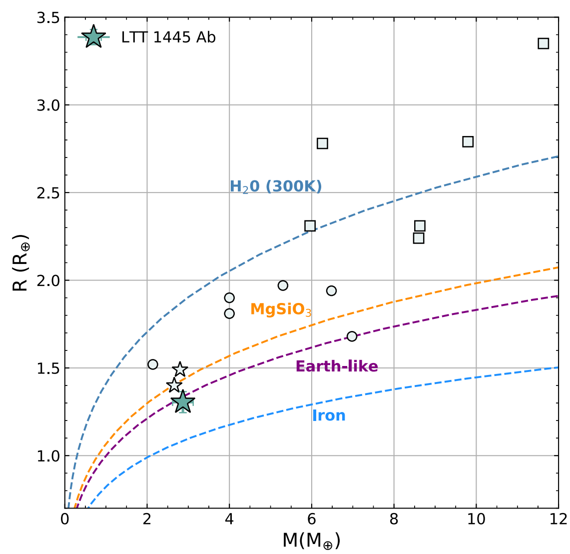

Figure 3. Mass−radius diagram for future targets of interest along with LTT 1445 Ab (blue star). The star markers correspond to objects below the radius valley (R < 1.5 $R_\oplus$). The circle markers correspond to objects within the radius valley (1.5 < $R_\oplus$ < 2.0). The square markers are those targets above the radius valley ($R_\oplus$ > 2.0). LTT 1445 Ab falls near the composition curve corresponding to an Earth-like planet. The curves are interior structure models of 100 per cent water (dark blue), 100 per cent magnesium silicate rock (orange), 33 per cent iron plus 67 per cent rock (purple) (i.e. Earth-like), and 100 per cent iron (light blue). The values are from Zeng et al. (2019).

We also aim to explore whether or not a Hycean and Haber world can be distinguished using the bulk properties of LTT 1445 Ab and *Twinkle.* We use the bulk properties (M_p and R_p) of LTT 1445 Ab to constrain the interior composition and to assist with distinguishing a cold Haber world from a Hycean world.

As shown in Section 4.1, our interior composition analysis indicates that LTT 1445 Ab is likely not a Hycean world. As a result, we model LTT 1445 Ab as a cold Haber world.

4.1 Composition of LTT 1445 Ab

With a planet mass and radius uncertainty of 9 per cent and 5 per cent (Winters et al. 2021), LTT 1445 Ab is among the best characterized small planets. Such precision in its mass and radius allows us to place constraints on its composition. In Fig. 3, we show theoretical mass–radius composition curves (Zeng et al. 2019) and place LTT 1445 Ab in the context of other small exoplanets from the literature that are within *Twinkle's* field of view. LTT 1445 Ab falls near the Earth-like composition curve of 67 per cent magnesium silicate and 33 per cent iron, suggesting that it is likely a rocky planet without a substantial water layer.

We further explore the interior composition of LTT 1445 Ab and calculate its core mass fraction (CMF) using the EXOPLEX software (Unterborn et al. 2018; Schulze et al. 2020), which solves the equations of planetary structure and calculates a CMF for a given planet mass and radius. EXOPLEX assumes a two-layer planet consisting of an iron core and a pure, magnesium silicate ($MgSiO_3$) mantle. Assuming the planet mass and radius from Winters et al. (2021) of $R_p = 1.304^{+0.067}_{-0.060}$ $R_\oplus$ and $M_p = 2.87 \pm 0.25$ $M_\oplus$, we obtain a CMF of CMF $= 0.42^{+0.18}_{-0.17}$. This value is consistent with the value of CMF $= 0.42 \pm 0.28$ reported by Winters et al. (2021), calculated using the semi-empirical relations of Zeng & Jacobsen (2017). As an alternative check on the CMF, we calculated the core radius fraction using HARDCORE (Suissa, Chen & Kipping 2018), and obtain a value of CRF $= 0.67 \pm 0.14$, which can be easily converted to a CMF using the empirical relations from Zeng, Sasselov & Jacobsen (2016). From

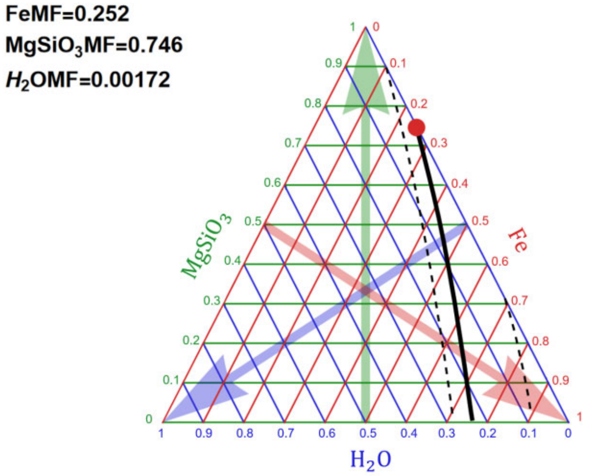

Figure 4. Ternary diagram showing the possible compositions of LTT 1445 Ab using the models from Zeng & Sasselov (2013). The red dot denotes relative mass fractions of the three layers (Fe, $MgSiO_3$, H_2O). The solid black line represents all the possible mass combinations of these layers allowed by the planet's mass and radius, and the black dashed lines represent the uncertainties. The best-fitting solution indicates that LTT 1445 Ab has a negligible fraction of water, likely ruling it out as a Hycean world.

that, we obtain CMF $= 0.45 \pm 0.08$, which is consistent with the value from EXOPLEX.

We also investigated the interior composition of LTT 1445 Ab using the theoretical models of Zeng & Sasselov (2013). In these models, the planet consists of three layers: an iron core, a magnesium silicate mantle ($MgSiO_3$), and a water layer overlaying the mantle and iron core. Fig. 4 shows a ternary diagram with the range of compositions allowed within the uncertainties of the mass and radius of LTT 1445 Ab. We obtain an iron mass fraction of 0.252, a silicate mass fraction of 0.746, and a water mass fraction of 0.002. Some of the other possible solutions along the black line are disfavoured for theoretical reasons. For example, a planet consisting purely of water and iron is physically unlikely (∼25 per cent H_2O and ∼75 per cent Fe core), e.g. Marcus et al. (2010). The best-fitting solution indicates that LTT 1445 Ab is likely a dry planet, i.e. not a Hycean world as proposed by Madhusudhan et al. (2021). According to Madhusudhan et al. (2021), a typical Hycean planet would have an H_2-rich atmosphere and a H_2O layer with a water mass fraction between 10 per cent and 90 per cent, and iron core + mantle with at least a 10 per cent mass fraction.

The discrepancy between the classification of Madhusudhan et al. (2021) and ours is probably due to the lower mass they used of $\sim 2.2\,M_{\oplus}$. The revised larger mass with lower uncertainty reported by Winters et al. (2021) leads to a higher density and a more Earth-like, rocky composition, thus ruling out the presence of a thick ocean layer.

4.2 Simulating a cold Haber world spectrum

We use the PYTHON package, PETITRADTRANS[4] (Mollière et al. 2019), to simulate the planetary atmosphere for transmission spectroscopy. The reference pressure is set to $P_0 = 1.0$ bar (Hu, Seager & Bains 2012; Seager et al. 2013a, 2013b) for a cold Haber world scenario, which is modelled after an Earth-size and Earth mass habitable rocky exoplanet.

[4]https://gitlab.com/mauricemolli/petitRADTRANS

Table 3. Species used for petitRADTRANS to generate synthetic spectra with 90 per cent H_2 and 10 per cent N_2 atmosphere for a cold Haber world.

Species	VMR[a]	MMR
H_2O	9.17×10^{-7}	3.62×10^{-6}
CO_2	2.90×10^{-9}	2.81×10^{-8}
CH_4	2.90×10^{-8}	1.02×10^{-7}
H_2	8.25×10^{-1}	3.62×10^{-1}
CO	9.17×10^{-10}	5.64×10^{-9}
OH	9.17×10^{-16}	3.42×10^{-15}
HCN	9.17×10^{-10}	5.44×10^{-9}
NH_3	3.66×10^{-6}	1.37×10^{-5}
N_2 [b]	9.17×10^{-2}	5.64×10^{-1}
He	8.25×10^{-2}	7.25×10^{-2}

[a]We adopt the mixing ratios for gases other than N_2 or H_2 (Seager et al. 2013b), assuming no major change in the chemistry. [b]N_2 has no rotational–vibrational transitions, so there are no signatures observable at infrared wavelengths, so this feature is not available in petitRADTRANS but is used to determine the mean molecular weight of the atmosphere.

We consider an isothermal atmosphere with an upper and lower pressure limit of 10^{-9} and 10^2 bar. The model atmosphere is divided into 100 layers with an equal logarithmic pressure spacing. The large pressure range is chosen to encompass the range of pressures that contribute to the flux for a large range of NH_3 concentration. For example, at 4.0 ppm of NH_3 concentration, the most flux is contributed from pressure range from 10 bar to 1 mbar. At another extreme NH_3 concentration that we consider at 40 000 ppm, the flux is mostly contributed by pressures from 1 bar to 10 nbar. In most cases, we do not need to be concerned about the lack of cross sections at extremely low pressures and the non-LTE effect at high pressures.

We modelled the performance of *Twinkle* using TWINKLERAD an adapted version of the radiometric tool described in Mugnai et al. (2020). We note that, due to the ongoing detailed design work, there are currently significant performance margins built-in to this simulator.

We employ the same methods used in Phillips et al. (2021) to calculate the atmospheric composition for a cold Haber world. We use the values in Table 3 to build the synthetic spectrum with a base atmosphere of 90 per cent H_2 and 10 per cent N_2 along with other trace species as in Table 3.

The opacity sources are H_2O (Polyansky et al. 2018),[5] CH_4 (Yurchenko et al. 2017), CO_2 (Yurchenko et al. 2020), CO (Burch et al. 1969), HCN (Barber et al. 2014), NH_3 (Coles, Yurchenko & Tennyson 2019), and OH (Brooke et al. 2016), H_2 (Hartmann et al. 2002), and collision-induced absorption due to H_2–H_2 and H_2–He (Richard et al. 2012).

As in Phillips et al. (2021), the VMRs from Seager et al. (2013b) are summed and normalized by dividing by the summation so the total volume mixing ratio (VMR) adds to 1.0. A fixed number of 25 transits is set to determine NH_3 is detectable. TAUREX 3 (Al-Refaie et al. 2021) is used to bin the spectra to the resolution of *Twinkle*. The resolution of *Twinkle* Channel 0 (0.5–2.4 μm) and Channel 1 (2.4–4.5 μm) are $R = 70$ and $R = 50$, respectively. Synthetic noise is added using a random Gaussian distribution. The S/N detection metric and threshold (equations 2 and 3; $\langle S/N \rangle \geq 3\sigma$) is the same as

[5]In our retrieval analysis (Section 6) using PETITRADTRANS, H_2O is reported as $H_2O_{\rm Exomol}$. This line list for $H_2^{16}O$ is the most complete high-accuracy line list for water (Polyansky et al. 2018).

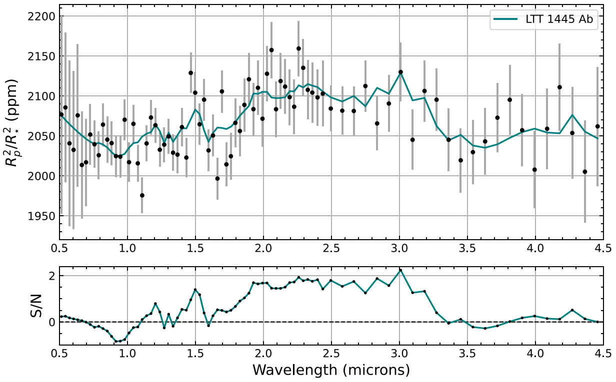

Figure 5. *Top:* Simulated cold Haber world transmission spectra of LTT 1445 Ab with 25 transits. Low mean molecular weight case ($\mu \sim 4.5$). *Bottom:* The corresponding S/N for 25 transits of LTT 1445 Ab.

in Phillips et al. (2021). The simulation for 25 transits with *Twinkle* with the corresponding S/N is shown in Fig. 5.

$$S/N = \frac{(R_\mathrm{p}/R_\star)^2 - \overline{(R_\mathrm{p}/R_\star)^2}}{\sigma_{(R_\mathrm{p}/R_\star)^2}}, \tag{2}$$

where $(R_\mathrm{p}/R_\star)^2$ is the transmission signal from PETITRADTRANS, $\overline{(R_\mathrm{p}/R_\star)^2}$ is median of the transmission signal from PETITRADTRANS, and $\sigma_{(R_\mathrm{p}/R_\star)^2}$ is the uncertainty.

For the final S/N determination, we follow Phillips et al. (2021) and use the following equation:

$$< S/N >= \sqrt{\sum_i (S/N)_i^2}, \tag{3}$$

where i indicates NH_3 wavelength features at 1.5, 2.0, 2.3, and 3.0 µm. For each NH_3 wavelength feature we find the data points around the central wavelength for signal and adjacent data points as a baseline to compute the S/N (for more details about the approach used, see Phillips et al. 2021).

4.3 Can *Twinkle* distinguish a cold Haber world from a Hycean world?

While LTT 1445 Ab is not in the traditional habitable zone of its star (Winters et al. 2019), it is considered as a candidate Hycean world where a liquid ocean may exist underneath a H_2-dominated atmosphere. In a Hycean world scenario, LTT 1445 Ab lies in the Hycean habitable zone. The Hycean habitable zone is defined as regions corresponding to the maximum irradiation that allows for habitable conditions at the surface of the ocean (Madhusudhan et al. 2021). For a Hycean world, Madhusudhan et al. (2021) consider H_2O, CH_4, and NH_3 as potentially abundant molecules in a H_2-based atmosphere. The question remains if we can use *Twinkle* to distinguish between a Hycean world and a cold Haber world. This is an important question because detecting NH_3 needs to be put into larger context of which world it belongs to. For a cold Haber world, NH_3 is regarded as a biosignature (Seager et al. 2013a), however, NH_3 detection may be unrelated to life in a Hycean world but none the less is a critical chemical species in the atmosphere (Madhusudhan et al. 2021).

In order to distinguish between two worlds, we first simulate *Twinkle* observations of a Hycean world for LTT 1445 Ab. Then, we compare the simulated data with that of a cold Haber world and evaluate the quality of the fit using the reduced χ^2 statistic. Below we detail the two steps.

Table 4. Species used for PETITRADTRANS to generate synthetic Hycean-world spectra atmosphere, adopted from Madhusudhan et al. (2021).

Species	VMR	MMR
H_2O	7.26×10^{-2}	2.39×10^{-1}
CH_4	5.00×10^{-4}	1.06×10^{-3}
H_2	6.54×10^{-1}	2.39×10^{-1}
NH_3	1.30×10^{-4}	2.94×10^{-4}
He	8.25×10^{-2}	7.25×10^{-2}

We simulate the Hycean-case scenario for LTT 1445 Ab by adopting the volume mixing ratios provided in Madhusudhan et al. (2021). In their work, they assume a volume mixing ratio of 0.1, 5.0×10^{-4}, and 1.3×10^{-4} for H_2O, CH_4, and NH_3, respectively. These values are based on the archetypal model for K2-18 b, a candidate Hycean world.

Similar to Madhusudhan et al. (2021), we assume a solar abundance for He and collision-induced absorption from H_2–H_2 and H_2–He. We then convert these values to mass mixing ratios (Table 4). We use these mass mixing ratios as input to PETITRADTRANS and simulate the atmosphere. The pressure bar is set to $P_0 = 1.0$ bar, low resolution mode is used, and an 424 K isothermal atmosphere is assumed.

To quantify if a cold Haber world and Hycean world can be distinguished with *Twinkle* spectroscopically, we implement a χ^2 statistical test (equation 4), and sample the PETITRADTRANS spectrum to a common wavelength grid.

We match the scaling between the Hycean world spectrum and the cold Haber world spectrum by applying a multiplicative factor to the Hycean world spectrum and minimizing the difference across the wavelength grid. We do this to account for the vertical shift between the two spectra due to the uncertainty in the solid surface radius of the planet that can affect the transmission signal. We then calculate the reduced χ^2 statistic, $\chi_\nu^2 \equiv \chi^2/\nu$, where ν represents the number of degrees of freedom, which corresponds to the numbers of wavelength bins for *Twinkle* (i.e. 83) minus the number of free parameters (i.e. 1)

$$\chi^2 = \sum_{i=0}^{n-1} \frac{(\mathrm{Hycean}_i - \mathrm{Haber}_i)^2}{\sigma_i^2}. \tag{4}$$

In equation (4), subscript i is the wavelength index to match the Twinkle wavelength grid, Hycean indicates the spectrum for a Hycean world, Haber indicates the spectrum for a cold Haber world, and σ is the expected noise for 25 transits observed by *Twinkle*. Based on this metric we find a $\chi_\nu^2 = 1.00$, indicating that spectroscopically *Twinkle* would not be able to distinguish a cold Haber world from a Hycean world (Fig. 6).

For a more robust statistical analysis to distinguish a cold Haber world from a Hycean world for LTT 1445 Ab, we follow Kass & Raftery (1995) and use the Bayesian evidence to compute the logEvidence or logEv. We use the following selection criterion from Kass & Raftery (1995) to distinguish between two models, with evidence again the lower Δ logEv as:

(i) $0 < \Delta\mathrm{logEv} < 0.5$: no preference worth mentioning
(ii) $0.5 < \Delta\mathrm{logEv} < 1.0$: positive
(iii) $1 < \Delta\mathrm{logEv} < 2.0$: strong
(iv) $\Delta\mathrm{logEv} > 2.0$: very strong

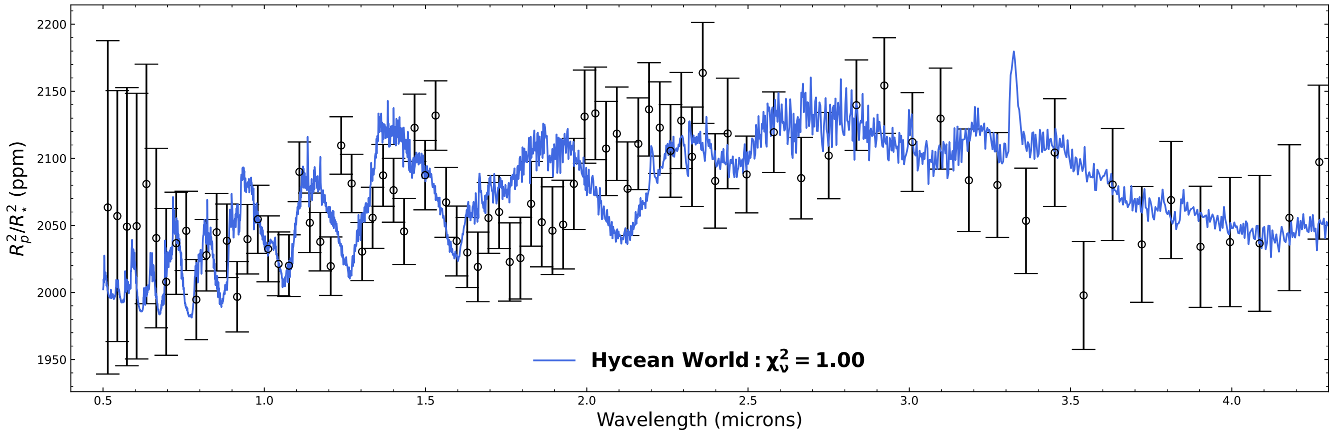

Figure 6. Simulated transmission spectra of LTT 1445 Ab as a cold Haber world with 90 per cent H_2 (black points with error bars) compared to a theoretical spectrum of a Hycean world (blue).

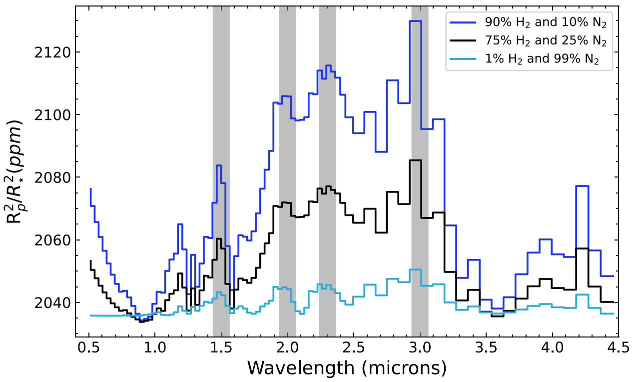

Figure 7. Modelled transmission spectra of LTT 1445 Ab showing various atmospheric compositions. The lines represent different hydrogen dominated scenarios: a H-rich atmosphere (90 per cent H_2 and 10 per cent N_2), a H-poor atmosphere (1 per cent H_2 and 99 per cent N_2), and a H-intermediate atmosphere (75 per cent H_2 and 25 per cent N_2). Contributing NH_3 features are shown in grey.

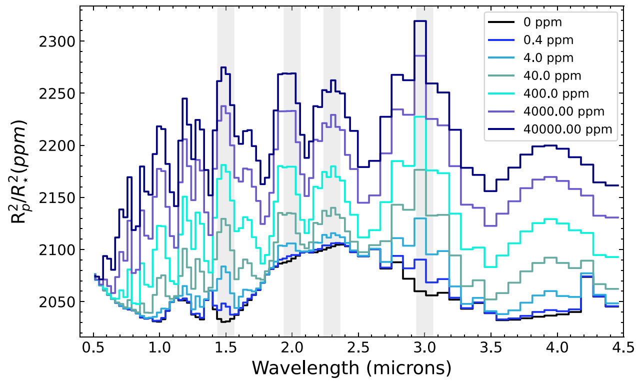

Figure 8. Theoretical transmission spectra of LTT 1445 Ab with varying level of ammonia concentration, 0, 0.4, 4.0, 40, 400, 4000, and 40 000 ppm. Contributing NH_3 features are shown in light grey.

To determine the ability to distinguish between two models with *Twinkle*, we run a retrieval analysis with PETITRADTRANS for the following four cases: (1) a forward model building upon a cold Haber world scenario with an input spectrum of a cold Haber world (Haber–Haber), (2) a Hycean world forward model building upon a Hycean world scenario with an input spectrum of a cold Haber world (Haber–Hycean), (3) a Hycean world forward model with an input spectrum of Hycean model (Hycean–Hycean), and lastly (4) a Hycean forward model with an input spectrum of a cold Haber world scenario (Hycean–Haber).

Table 5 lists all tested models as well as their Δ logEv. For the first set of retrieval with the cold Haber world as the input spectrum, we find that the difference in the Δ logEv has no preference worth mentioning. This indicates that given the scenario that LTT 1445 Ab is cold Haber world, retrieval analysis would not be able to distinguish between a cold Haber world and a Hycean world. For the second set of retrievals, with the input as a Hycean world, we find that the Δ logEV has a preference. This indicates that if LTT 1445 Ab was indeed a Hycean world, a retrieval analysis might be able to slightly distinguish between a Hycean world and cold Haber world, but the evidence is not very strong.

We find, through a χ^2_ν and a Δ logEV statistical analysis and comparison, that *Twinkle* would not be able to distinguish between a cold Haber world and Hycean world. However, given our composition analysis of LTT 1445 Ab Section 4.1, we model LTT 1445 Ab as a cold Haber world given that LTT 1445 Ab is likely not a Hycean world.

5 MAIN RESULTS ON NH_3 DETECTION

5.1 What fraction of hydrogen is *Twinkle* sensitive to?

Small planets ($R \lesssim 1.6\,R_\oplus$) have less gravity and can be prone to losing their atmospheres. Atmospheric loss can be due to either core powered atmospheric mass-loss (Gupta & Schlichting 2021 and references therein) and/or photoevaporation atmospheric mass-loss (e.g. Lopez & Fortney 2013; Owen & Wu 2017; Ginzburg, Schlichting & Sari 2018; Diamond-Lowe et al. 2022). The lowest mass of an exoplanet known to host a voluminous H_2/He atmosphere is $\sim 2\,M_\oplus$, despite this it is possible that they may exist at even lower masses (Owen et al. 2020).

We explore the scenario of likely H_2 mass-loss of LTT 1445 Ab and see which lower limit fraction of hydrogen *Twinkle* is sensitive to. We follow Miller-Ricci et al. (2008), Chouqar et al. (2020), and Phillips et al. (2021) and consider the following scenarios: a hydrogen-rich atmosphere (90 per cent H_2 and 10 per cent N_2), a

Table 5. Δ logEv and logEvidence.

Model	Bayesian/logEvidence	Δ logEv
Haber–Haber	– 45.44	0.16
Haber–Hycean	– 45.28	0.00
Hycean–Hycean	– 108.14	0.00
Hycean–Haber	– 109.17	1.02

Table 6. Average S/N of major NH_3 transmission features for LTT 1445 Ab transmission spectroscopy for different atmospheric compositions.

LTT 1445 Ab	Ammonia feature (μm)	S/N (σ)	Total <S/N> (σ)
H-rich	1.5	1.13	3.10
	2.0	1.56	
	2.3	1.75	
	3.0	1.67	
H-intermediate	1.5	0.69	1.79
	2.0	0.89	
	2.3	0.99	
	3.0	0.97	
H-poor	1.5	0.61	1.08
	2.0	0.47	
	2.3	0.49	
	3.0	0.57	

hydrogen-poor atmosphere (1 per cent H_2 and 99 per cent N_2), and a hydrogen-intermediate atmosphere (75 per cent H_2 and 25 per cent N_2)(Fig. 7).

We determine the effects of a reduction in hydrogen in the atmosphere on the detection of ammonia. For LTT 1445 Ab, we find that the atmosphere would need to be H-rich (90 per cent H_2) for NH_3 to be detectable by *Twinkle* at a 3σ level (Table 6).

5.2 Other factors that impact NH_3 detection: ammonia concentration and clouds

The lifetime and concentration of NH_3 in a H_2 dominated atmosphere has been previously studied (e.g. Tsai et al. 2021; Ranjan et al. 2022). We explore how the concentration of ammonia affects the S/N detection in the atmosphere of LTT 1445 Ab.

Tsai et al. (2021) explored the evolution of the column mixing ratio for NH_3 for an atmosphere with 1-bar surface with a planet around a quiet M-dwarf host and a planet around an active M-dwarf host. They found that for a quiet M-dwarf, the mixing ratio of NH_3 can vary from $\sim 10^{-2}$ to 10^{-4} given a span of 10^3 to 10^8 yr. In contrast, the atmospheric NH_3 mixing ratio can vary from $\sim 10^{-2}$ to 10^{-10} around an active M-dwarf over the same span of time.

A recent study by Ranjan et al. (2022) found that an Earth-sized planet with an H_2-dominated atmosphere can enter photochemical runaway of NH_3 if the net surface production of NH_3 $\geq 2 \times 10^{10}\,\mathrm{cm^{-2}\,s^{-1}}$. Photochemical runaway occurs of NH_3 occurs when the production rate of NH_3 exceeds the photochemical destruction rate. Once in photochemical runaway, the mixing ratio of NH_3 can increase beyond 10^{-6} with concentrations up to 70 ppmv of NH_3.

We consider different levels of NH_3 atmospheric concentration that are within the theoretical range as predicted by Tsai et al. (2021). We find that a baseline of 4.0 ppm of NH_3 is needed to be detected by *Twinkle* at a 3σ level. Notably, beyond a concentration of 400 ppm

Table 7. NH_3 transmission features for LTT 1445 Ab transmission spectroscopy for varying concentrations of ammonia.

Concentration of NH_3	Ammonia feature (μm)	S/N (σ)	Total <S/N> (σ)
0.4 ppm	1.5	0.10	2.55
	2.0	1.52	
	2.3	1.73	
	3.0	1.08	
4.0 ppm	1.5	1.13	3.10
	2.0	1.56	
	2.3	1.75	
	3.0	1.67	
40 ppm	1.5	2.43	4.34
	2.0	1.92	
	2.3	1.98	
	3.0	2.30	
400 ppm	1.5	3.34	5.32
	2.0	2.33	
	2.3	2.22	
	3.0	2.59	
4000 ppm	1.5	4.15	6.62
	2.0	2.86	
	2.3	2.66	
	3.0	3.37	
40 000 pm	1.5	4.30	6.75
	2.0	2.94	
	2.3	2.67	
	3.0	3.37	

NH_3, the S/N is nearly constant (Table 7 & Fig. 8.). We find that for the concentration levels of NH_3 at 4000 and 40 000 ppm the S/N is nearly indistinguishable and do not continue a linear increase and plateaus. While beyond the scope of this work, we note that the apparent ammonia plateau would be worthwhile to investigate for future work.

Additionally, we study the impact of clouds on NH_3 detection. Clouds can mute spectral features in hydrogen-rich atmospheres and impact transmission spectroscopy observations (e.g. Kitzmann et al. 2010; Benneke et al. 2019). There is evidence for the presence of clouds in super-Earths and mini-Neptunes (e.g. Knutson et al. 2014; Kreidberg et al. 2014; Lothringer et al. 2018; Helling 2019) and in our Solar system (Max et al. 2003; Coulter, Barnes & Fortney 2022; Yin et al. 2022). We use `petitRADTRANS` to model the effects of clouds by setting a grey cloud deck at 1.0, 0.1, and 0.01 bar (Table 8). We choose these grey cloud deck levels because condensation curves for temperate exoplanets indicate that H_2O should condense at pressures below 1.0 bar and form clouds (e.g. Lodders 2003; Marley & Robinson 2015; Tinetti et al. 2018). We find that the presence of clouds even at 1.0 bar lowers the S/N of previously observable NH_3 features to below 3σ.

Table 8. Average S/N of major NH_3 transmission features for LTT 1445 Ab transmission spectroscopy for varying cloud decks with a H-rich atmosphere.

LTT 1445 Ab	Ammonia feature (μm)	S/N (σ)	Total <S/N> (σ)
Cloud deck at 0.01 bar	1.5	0.03	0.15
	2.0	0.05	
	2.3	0.06	
	3.0	0.12	
Cloud deck at 0.1 bar	1.5	0.24	0.91
	2.0	0.36	
	2.3	0.52	
	3.0	0.59	
Cloud deck at 1.0 bar	1.5	0.96	2.80
	2.0	1.42	
	2.3	1.61	
	3.0	1.51	

6 ATMOSPHERIC RETRIEVAL RESULTS

In this section, we investigate how the abundance of NH_3 can be constrained using retrieval analysis. We use PETITRADTRANS (Mollière et al. 2020) and PYMULTINEST (Buchner et al. 2014) to sample the posteriors. PYMULTINEST is the PYTHON version of MULTINEST for nested sampling (Feroz, Hobson & Bridges 2009). In PYMULTINEST, we use 2000 live points. Modelling parameters, priors, and retrieval results can be found in Table 10.

6.1 Atmospheric retrieval setup

We use the simulated cold Haber world *Twinkle* data for LTT 1445 Ab as the input (Fig. 5 & Table 3). To model the simulated data, we use with the following free parameters: surface gravity, planet radius, temperature for the isothermal atmosphere, cloud deck pressure, and mass mixing ratios for different species that are being considered.

We conduct retrievals for two model setups: (1) a clear atmosphere and (2) an atmosphere with clouds that are parametrized by a grey cloud deck pressure to assess the impact on clouds on the retrieval.

6.2 Cloud-free and fixed minor species

In this case, we use the simulated data for the cloud-free low-mean molecular weight case for LTT 1445 Ab (Fig. 5). We also assume an abscence of a clouds in our retrieval. Given the low abundance/low signal of species other than NH_3, H_2O, and CH_4, we fix these species as these species would not be readily detectable. Additionally as with the work in Phillips et al. (2021), we want to check if NH_3 and H_2O can be measured given their overlapping features.

6.2.1 Flat priors on log (g_{pl}) and planetary radius (R_{pl})

We apply a flat prior for the surface gravity of the planet and planet radius. As shown in Fig. 9, NH_3 and H_2O can be detected in our retrieval, and their abundances are within 1σ from the input values. We note that the planetary radius and log (g) are poorly constrained in the case of flat priors. Given that the radius and mass and thus the surface gravity are more precisely constrained by observations (Winters et al. 2021) we introduce Gaussian priors for these values to test the result of our retrieval analysis.

6.2.2 Gaussian priors on log (g_{pl}) and planetary radius (R_{pl})

We now consider a retrieval case with Gaussian priors on the log (g) and planetary radius. We apply a Gaussian prior of 3.217 ± 0.05 dex

Table 9. Bayesian model comparison for species of interest for Cold Haber World Scenario for LTT 1445 Ab.

Retrieval model	Retrieved model parameters	Evidence $\log_{10} \mathcal{Z}$	Bayes factor $B_i = \mathcal{Z}_0/\mathcal{Z}_i$	ln (Bayes factor) ln(B_i)	'Sigma' significance[b] σ
Full parameter space	all[a]	-45.285	Reference	...	
H_2O removed	all – H_2O	−45.516	$B_{H_2O} = 1.702$	0.531	<2.0
NH_3 removed	all – NH_3	−47.778	$B_{NH_3} = 311.172$	5.740	>5.0
CH_4 removed	all – CH_4	−44.786	$B_{CH_4} = 0.316$	−1.148	<2.0

[a]The full parameters as described in Section 6.3 and Table 10.
[b]The general upper limit on the 'sigma' significance from table 2 in Benneke & Seager (2013), which is adapted from Trotta (2008).

Table 10. Parameters used in retrieval, their priors, input, and retrieved values.

Parameter	Unit	Type	Lower or mean	Upper or std	Input	Retrieved: Fixed [Gaussian priors]	Retrieved: Fixed [flat priors]	Retrieved: Free [Gaussian priors]
Surface gravity (*logg*)	cgs	Uniform	2.0	5.0	3.217	...	$3.69^{+0.24}_{-0.42}$	...
Surface gravity (*logg*)	cgs	Gaussian	3.217	0.050	3.217	$3.23^{+0.05}_{-0.05}$	...	$3.22^{+0.04}_{-0.04}$
Planet radius (R_P)	$R_{Jupiter}$	Uniform	0.1	0.5	0.1164	...	$0.30^{+0.08}_{-0.20}$	...
Planet radius (R_P)	$R_{Jupiter}$	Gaussian	0.1164	0.005	0.1164	$0.12^{+0.00}_{-0.00}$	...	$0.12^{+0.00}_{-0.00}$
Temperature (T_{iso})	K	Log-uniform	10	810	424	370^{+70}_{-62}	481^{+160}_{-181}	360^{+69}_{-60}
H_2O mixing ratio ($\log(mr_{H_2O})$)	...	Log-uniform	−12	0	−5.44	$-5.53^{+0.88}_{-3.39}$	$-5.81^{+1.09}_{-3.65}$	$-5.56^{+0.94}_{-3.39}$
CO mixing ratio ($\log(mr_{CO})$)	...	Log-uniform	−12	0	−8.25	fixed	fixed	$-7.70^{+2.99}_{-2.74}$
CO_2 mixing ratio ($\log(mr_{CO_2})$)	...	Log-uniform	−12	0	−7.55	fixed	fixed	$-9.01^{+2.00}_{-1.94}$
CH_4 mixing ratio ($\log(mr_{CH_4})$)	...	Log-uniform	−12	0	−6.99	$-7.58^{+1.71}_{-2.84}$	$-7.96^{+1.89}_{-2.60}$	$-7.73^{+1.82}_{-2.71}$
OH mixing ratio ($\log(mr_{OH})$)	...	Log-uniform	−12	0	−14.47	fixed	fixed	$-7.76^{+2.77}_{-2.71}$
NH_3 mixing ratio ($\log(mr_{NH_3})$)	...	Log-uniform	−12	0	−4.86	$-4.93^{+0.34}_{-0.37}$	$-5.02^{+0.37}_{-0.48}$	$-4.96^{+0.36}_{-0.39}$
HCN mixing ratio ($\log(mr_{HCN})$)	...	Log-uniform	−12	0	−8.27	fixed	fixed	$-7.97^{+2.40}_{-2.55}$
$(R_p/R_\star)^2$ shift (Δ_y)	ppm	Uniform	−100	100	0	0.0009 ± 0.00012	-0.0107 ± 0.0074	0.0009 ± 0.00012

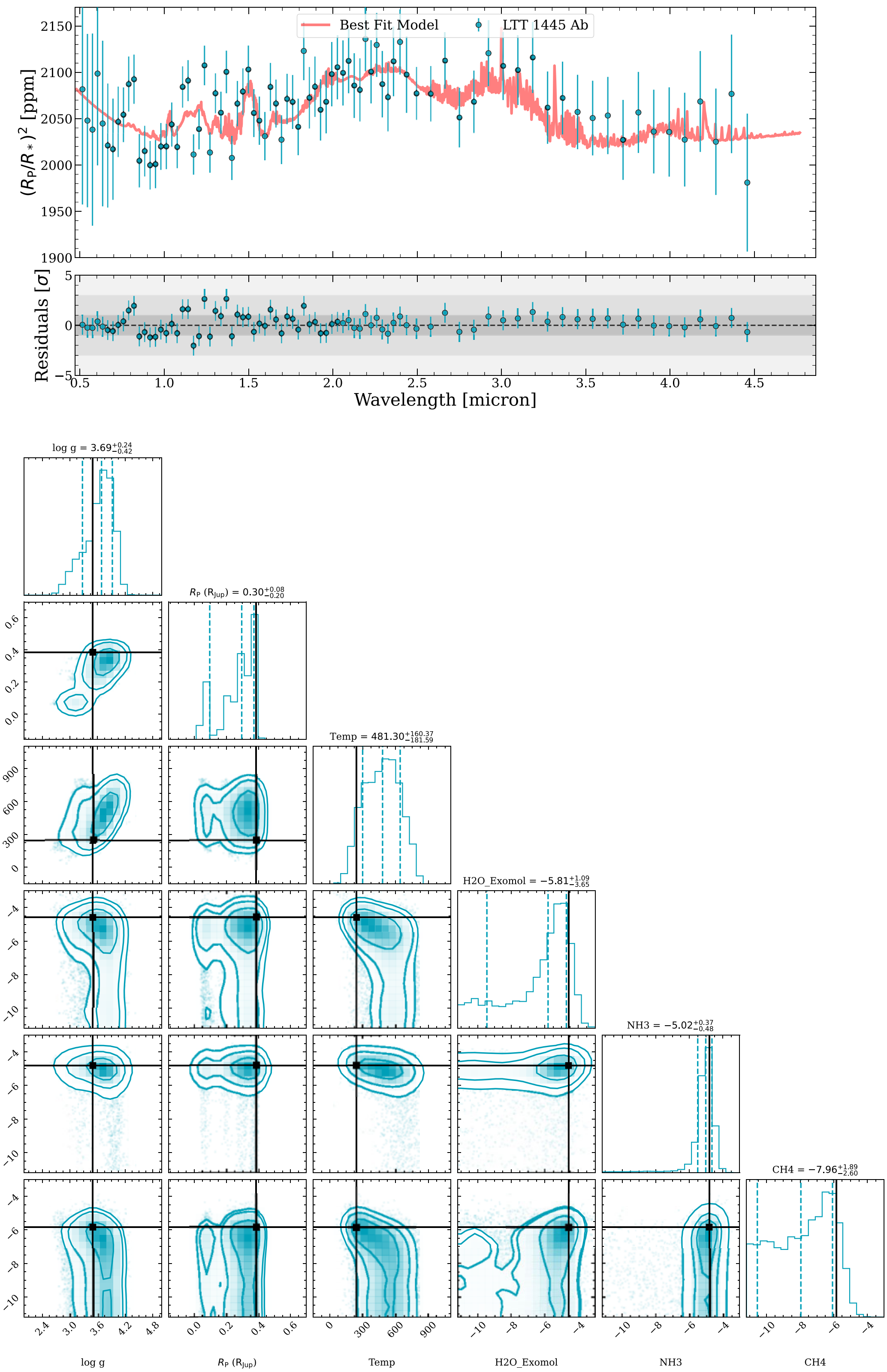

Figure 9. *Top:* Simulated *Twinkle* data versus the retrieved model with flat priors for the surface gravity (log g) and planet radius, and the residuals plotted below. *Bottom:* Posterior distribution as shown in a corner plot along with the true input values (black lines). Contours are at 1-σ, 2-σ, and 3-σ from inside out.

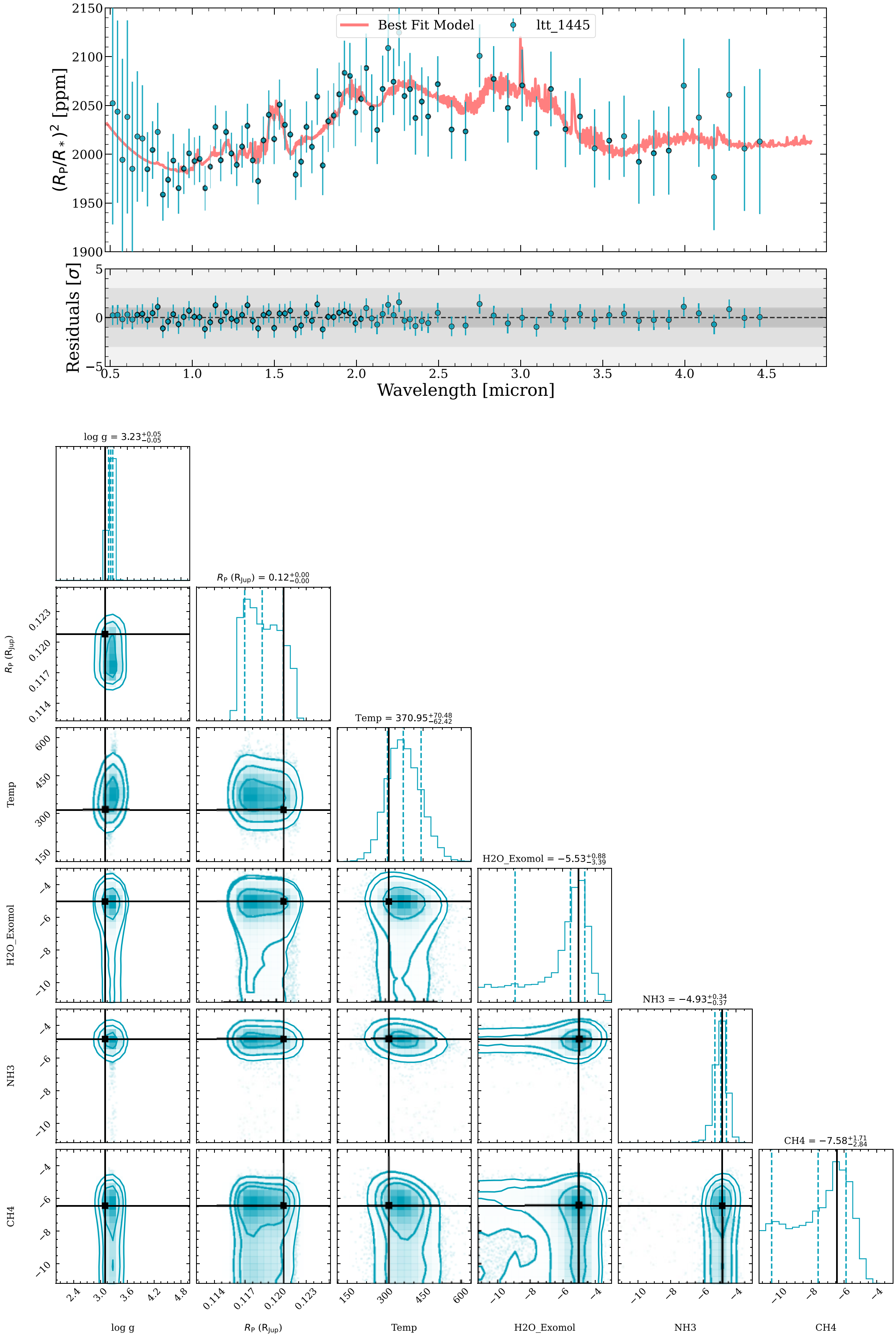

Figure 10. Same as Fig. 9 but with Gaussian priors for the surface gravity (log *g*) and planet radius.

for log (*g*) (surface gravity) and $0.1164 \pm 0.005\ R_{\rm Jup}$ for the planetary radius (Winters et al. 2021). In this case, log *g* and radius are more tightly constrained because of more constraining priors. Additionally, NH_3 and H_2O are within 1σ of their input values. The corner plot and accompanying spectra are shown in Fig. 10. Retrieval results can be found in Table 10.

To quantify the detection significance, we use similar methods as in Phillips et al. (2021). Given the 11 611 posterior samples, there

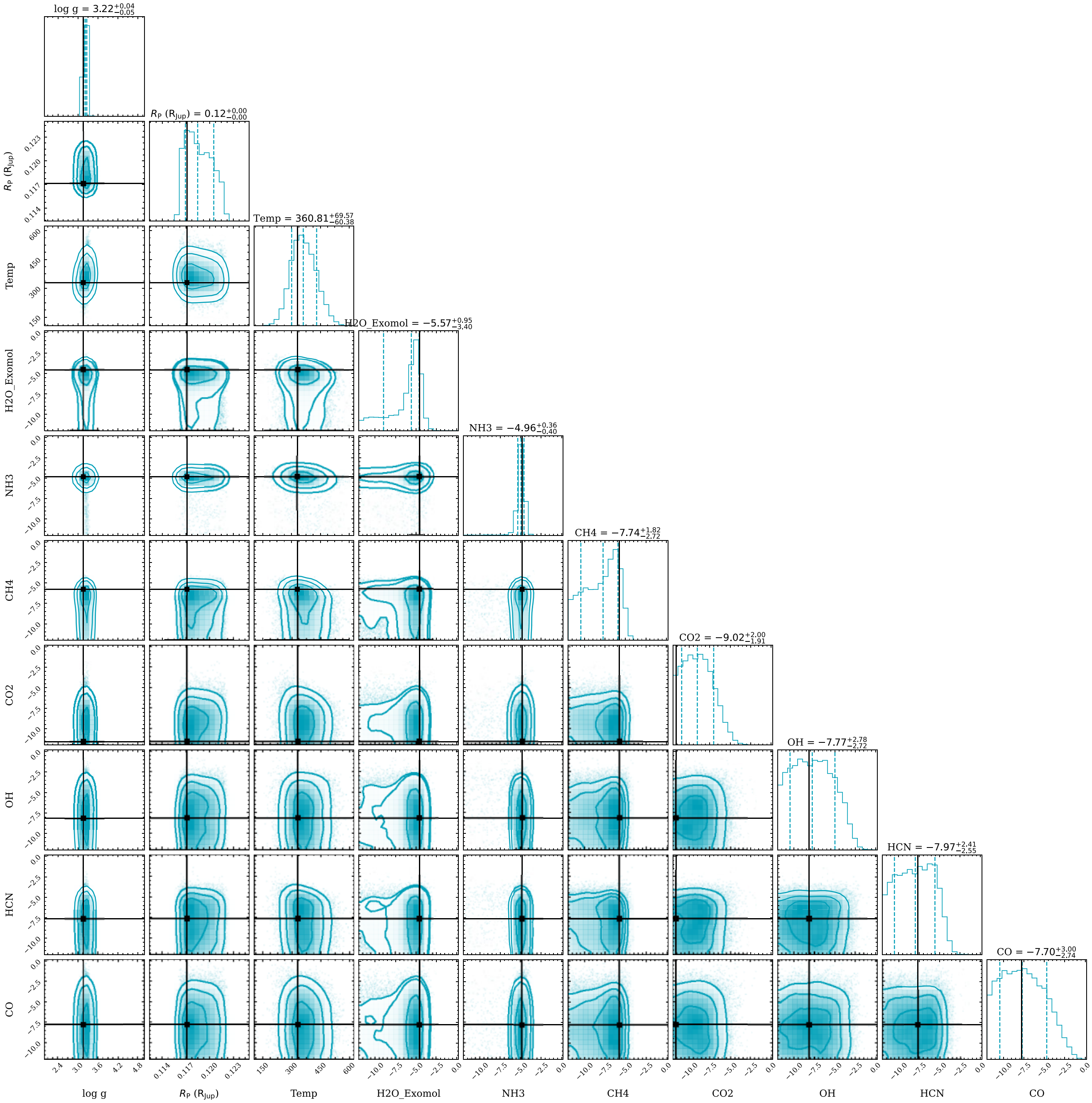

Figure 11. Corner plot for the full parameter set along with true values (black lines) that are used in generating the *Twinkle* data.

are ∼0.75 per cent that have a lower value than 10^{-8} mixing ratio for NH_3. The 10^{-8} mixing ratio threshold is chosen because below this value it is difficult for our retrieval code to constrain abundances (e.g. CH_4). The 0.75 per cent fraction translates to 2.6-σ assuming a normal distribution. This is consistent with the 3.1-σ detection significance from the SNR analysis in Section 5.

6.3 Cloud deck as a free parameter

Following Phillips et al. (2021), we also run a cloud-free retrieval analysis on the full parameter set that includes all minor species other than NH_3, H_2O, and CH_4. We are unable to constrain minor species with mixing ratio lower than 10^{-8}, but we can constrain NH_3 within 1σ of the input value. The results are in Table 10 and the corner plot is shown in Fig. 11.

6.3.1 Detection confidence for NH_3, H_2O, and CH_4

To assess the detection strength of species of interest (NH_3, H_2O, and CH_4) for LTT 1445 Ab as a cold Haber world scenario, we determine the respective Bayes factor for each species (Table 9). A Bayes factor higher than 1 ($B_m > 1$) favours the presence of an atmospheric component (Benneke & Seager 2013). Based on the

Bayes factors, we find that our retrieval is in favour of the presence of NH_3 ($B_{NH_3} = 311.172$) and H_2O ($B_{H_2O} = 1.702$), respectively and dis-favourable for a detection of CH_4 with a Bayes factor of $B_{CH_4} = 0.316$.

7 SUMMARY AND CONCLUSIONS

We model the terrestrial-like planet LTT 1445 Ab for the detection of the potential biosignature ammonia with the upcoming *Twinkle* mission. LTT 1445 Ab is modelled using PETITRADTRANS and TWINKLERAD. A baseline of 25 transits, 4.0 ppm concentration of NH_3, and a H-rich atmosphere is considered to determine whether NH_3 is detectable.

We explore the fraction of hydrogen needed in the atmosphere of LTT 1445 Ab for ammonia to be detectable (Section 5). We find that in order to detect NH_3, LTT 1445 Ab would need a significant portion of H_2 in the atmosphere ($H_2 = 90$ per cent). We also explore the effects on cloud decks and the concentration of NH_3 on the detectability of NH_3 in the atmosphere. We find that even the presence of a cloud deck at 1.0 bar would reduce the overall S/N to be lower than 3-σ for NH_3 detection. In addition, we find that a 4.0 ppm concentration of NH_3 is needed to be detectable by *Twinkle*.

Interior composition analysis indicates that LTT 1445 Ab is likely not a Hycean world. This planet is more consistent with a rocky planet without a substantial water mass fraction (Section 4.1). We demonstrate that, given the current performance modelling for *Twinkle* using TwinkleRad, *Twinkle* will not have the capabilities to distinguish between a cold Haber world and a Hycean world scenario (Section 4). Given the modelled spectra and the associated uncertainties, we find a $\chi^2_\nu = 1.00$, indicating that *Twinkle* cannot spectroscopically differentiate the two worlds. Comparative retrieval analysis also indicates that *Twinkle* cannot distinguish between a cold Haber world and Hycean world.

Lastly, we conduct atmospheric retrieval analysis (Section 6) which provides helpful insight into constraining NH_3 and H_2O given optimal conditions (i.e. a cloud-free atmosphere with low MMW). We use a Bayesian model comparison and find that NH_3 and H_2O are the only major atmospheric constituents that would be confidently detected at their concentration levels in a cold Haber world scenario.

This work demonstrates that *Twinkle* can provide useful characterization of promising potential smaller terrestrial-like planets to provide insights into potential biosignatures and atmospheric characterization.

ACKNOWLEDGEMENTS

This research has made use of the NASA Exoplanet Archive, which is operated by the California Institute of Technology, under contract with the National Aeronautics and Space Administration under the Exoplanet Exploration Program. This project received funding from the European Union's Horizon 2020 research and innovation programme under grant agreement no. 871149. JW acknowledges the support by the National Science Foundation under grant No. 2143400. Work by BSG was supported by the Thomas Jefferson Chair for Discovery and Space Exploration.

We thank the anonymous referee for their time providing helpful comments that improved the quality of this paper.

NASA's Astrophysics Data System Bibliographic Services together with the VizieR catalogue access tool and SIMBAD database operated at CDS, Strasbourg, France, were invaluable resources for this work. This publication makes use of data products from the Two Micron All Sky Survey, which is a joint project of the University of Massachusetts and the Infrared Processing and Analysis Center/California Institute of Technology, funded by the National Aeronautics and Space Administration and the National Science Foundation.

This work benefitted from involvement in ExoExplorers, which is sponsored by the Exoplanets Program Analysis Group (ExoPAG) and NASA's Exoplanet Exploration Program Office (ExEP). CP thanks the Rubin Observatory Legacy Survey of Space and Time (LSSTC) Data Science Fellowship Program, which is funded by LSSTC, NSF Cybertraining Grant #1829740, the Brinson Foundation, and the Moore Foundation; her participation in the programme has benefitted this work.

This research was supported by a Grant in Aid of Research from Sigma Xi, The Scientific Research Honor Society.

This work benefitted from the 2022 Exoplanet Summer Program in the Other Worlds Laboratory (OWL) at the University of California, Santa Cruz, a programme funded by the Heising–Simons Foundation.

This project was supported, in part, by funding from Two Sigma Investments, LP. Any opinions, findings, and conclusions or recommendations expressed in this material are those of the authors and do not necessarily reflect the views of Two Sigma Investments, LP. This work has made use of data from the European Space Agency (ESA) mission *Gaia* (https://www.cosmos.esa.int/gaia), processed by the *Gaia* Data Processing and Analysis Consortium (DPAC, https://www.cosmos.esa.int/web/gaia/dpac/consortium). Funding for the DPAC was provided by national institutions, in particular the institutions participating in the *Gaia* Multilateral Agreement.

DATA AVAILABILITY

The data underlying this article will be shared on reasonable request to the corresponding author.

REFERENCES

Al-Refaie A. F., Changeat Q., Waldmann I. P., Tinetti G., 2021, ApJ, 917, 37
Barber R. J., Strange J. K., Hill C., Polyansky O. L., Mellau G. C., Yurchenko S. N., Tennyson J., 2014, MNRAS, 437, 1828
Benneke B., Seager S., 2013, ApJ, 778, 153
Benneke B. et al., 2019, Nat. Astron., 3, 813
Borucki W. J. et al., 2010, Science, 327, 977
Brooke J. S., Bernath P. F., Western C. M., Sneden C., Afsar M., Li G., Gordon I. E., 2016, J. Quant. Spectrosc. Radiat. Transfer, 168, 142
Buchner J. et al., 2014, A&A, 564, A125
Burch D. E., Gryvnak D. A., Patty R. R., Bartky C. E., 1969, J. Opt. Soc. Am., 59, 267
Catling D. C. et al., 2018, Astrobiology, 18, 709
Chouqar J., Benkhaldoun Z., Jabiri A., Lustig-Yaeger J., Soubkiou A., Szentgyorgyi A., 2020, MNRAS, 495, 962
Coles P. A., Yurchenko S. N., Tennyson J., 2019, MNRAS, 490, 4638
Coulter D. J., Barnes J. W., Fortney J. J., 2022, ApJS, 263, 15
de Wit J. et al., 2016, Nature, 537, 69
Des Marais D. J. et al., 2002, Astrobiology, 2, 153
Des Marais D. J. et al., 2008, Astrobiology, 8, 715
Diamond-Lowe H., Berta-Thompson Z., Charbonneau D., Kempton E. M. R., 2018, AJ, 156, 42
Diamond-Lowe H., Berta-Thompson Z., Charbonneau D., Dittmann J., Kempton E. M. R., 2020, AJ, 160, 27
Diamond-Lowe H., Mendonca J. M., Charbonneau D., Buchhave L. A., 2022, AJ, 165, 169
Dittmann J. A. et al., 2017, Nature, 544, 333
Edwards B., Stotesbury I., 2021, AJ, 161, 266
Edwards B. et al., 2019, Exp. Astron., 47, 29
Edwards B. et al., 2021, AJ, 161, 44

Feroz F., Hobson M. P., Bridges M., 2009, MNRAS, 398, 1601
Fressin F. et al., 2013, ApJ, 766, 81
Fulton B. J. et al., 2017, AJ, 154, 109
Garcia L. J., Moran S. E., Rackham B. V., Wakeford H. R., Gillon M., de Wit J., Lewis N. K., 2022, A&A, 665, A19
Gillon M. et al., 2017, Nat. Astron., 1, 0056
Ginzburg S., Schlichting H. E., Sari R., 2018, MNRAS, 476, 759
Gupta A., Schlichting H. E., 2021, MNRAS, 504, 4634
Hartmann J. M., Boulet C., Brodbeck C., van Thanh N., Fouchet T., Drossart P., 2002, J. Quant. Spec. Radiat. Transfer, 72, 117
Helling C., 2019, Annu. Rev. Earth Planet. Sci., 47, 583
Hu R., Seager S., Bains W., 2012, ApJ, 761, 166
Hu R., Damiano M., Scheucher M., Kite E., Seager S., Rauer H., 2021, ApJ, 921, L8
Huang J., Seager S., Petkowski J. J., Ranjan S., Zhan Z., 2021, Astrobiology, 22, 171
Kass R. E., Raftery A. E., 1995, J. Am. Stat. Assoc., 90, 773
Kempton E. M. R. et al., 2018, PASP, 130, 114401
Kitzmann D., Patzer A. B. C., von Paris P., Godolt M., Stracke B., Gebauer S., Grenfell J. L., Rauer H., 2010, A&A, 511, A66
Knutson H. A., Benneke B., Deming D., Homeier D., 2014, Nature, 505, 66
Kreidberg L. et al., 2014, Nature, 505, 69
Léger A. et al., 2004, Icarus, 169, 499
Lodders K., 2003, ApJ, 591, 1220
Lopez E. D., Fortney J. J., 2013, ApJ, 776, 2
Lothringer J. D. et al., 2018, AJ, 155, 66
Madhusudhan N., Piette A. A. A., Constantinou S., 2021, ApJ, 918, 1
Marcus R. A., Sasselov D., Hernquist L., Stewart S. T., 2010, ApJ, 712, L73
Marley M. S., Robinson T. D., 2015, ARA&A, 53, 279
Max C. E. et al., 2003, AJ, 125, 364
Meadows V., Seager S., 2010, in Seager S., ed., Exoplanets. Univ. Arizona Press, Tucson, AZ, p. 441
Miller-Ricci E., Seager S., Sasselov D., 2008, ApJ, 690, 1056
Mollière P., Wardenier J. P., van Boekel R., Henning T., Molaverdikhani K., Snellen I. A. G., 2019, A&A, 627, A67
Mollière P. et al., 2020, A&A, 640, A131
Mugnai L. V., Pascale E., Edwards B., Papageorgiou A., Sarkar S., 2020, Exp. Astron., 50, 303
Nixon M. C., Madhusudhan N., 2021, MNRAS, 505, 3414
Noack L., Snellen I., Rauer H., 2017, Space Sci. Rev., 212, 877
Owen J. E., Wu Y., 2017, ApJ, 847, 29
Owen J. E., Shaikhislamov I. F., Lammer H., Fossati L., Khodachenko M. L., 2020, Space Sci. Rev., 216, 129
Phillips C., Wang J., Kendrew S., Greene T. P., Hu R., Valenti J., Panero W. R., Schulze J., 2021, ApJ, 923, 144
Polyansky O. L., Kyuberis A. A., Zobov N. F., Tennyson J., Yurchenko S. N., Lodi L., 2018, MNRAS, 480, 2597
Ramirez R. M., Levi A., 2018, MNRAS, 477, 4627
Ranjan S., Seager S., Zhan Z., Koll D. D. B., Bains W., Petkowski J. J., Huang J., Lin Z., 2022, ApJ, 930, 131
Richard C. et al., 2012, J. Quant. Spec. Radiat. Transfer, 113, 1276
Ricker G. R. et al., 2015, J. Astron. Telesc. Instrum. Syst., 1, 014003
Schulze J. G., Wang J., Johnson J. A., Unterborn C. T., Panero W. R., 2020, Planet. Sci. J., 2, 113
Seager S., Bains W., Hu R., 2013a, ApJ, 775, 104
Seager S., Bains W., Hu R., 2013b, ApJ, 777, 95
Selsis F. et al., 2007, Icarus, 191, 453
Stotesbury I. et al., 2022, Proc. SPIE Conf. Ser. Vol. 12180, Space Telescopes and Instrumentation 2022: Optical, Infrared, and Millimeter Wave. SPIE, Bellingham, p. 1218033
Suissa G., Chen J., Kipping D., 2018, MNRAS, 476, 2613
Thomas S. W., Madhusudhan N., 2016, MNRAS, 458, 1330
Tinetti G. et al., 2018, Exp. Astron., 46, 135
Trotta R., 2008, Contemp. Phys., 49, 71
Tsai S.-M., Innes H., Lichtenberg T., Taylor J., Malik M., Chubb K., Pierrehumbert R., 2021, ApJ, 922, L27
Unterborn C. T., Desch S. J., Hinkel N. R., Lorenzo A., 2018, Nat. Astron., 2, 297
Van Eylen V., Agentoft C., Lundkvist M. S., Kjeldsen H., Owen J. E., Fulton B. J., Petigura E., Snellen I., 2018, MNRAS, 479, 4786
Winters J. G. et al., 2019, AJ, 158, 152
Winters J. G. et al., 2021, AJ, 163, 168
Wunderlich F., Scheucher M., Grenfell J. L., Schreier F., Sousa-Silva C., Godolt M., Rauer H., 2020, A&A, 647, A48
Yin M., Wang P., Ni C., Hao W., 2022, Sci. Rep., 12, 14415
Yurchenko S. N., Amundsen D. S., Tennyson J., Waldmann I. P., 2017, A&A, 605, A95
Yurchenko S. N., Mellor T. M., Freedman R. S., Tennyson J., 2020, MNRAS, 496, 5282
Zeng L., Jacobsen S. B., 2017, ApJ, 837, 164
Zeng L., Sasselov D., 2013, PASP, 125, 227
Zeng L., Sasselov D., 2014, ApJ, 784, 96
Zeng L., Sasselov D. D., Jacobsen S. B., 2016, ApJ, 819, 127
Zeng L. et al., 2019, Proc. Natl. Acad. Sci. USA, 116, 9723

This paper has been typeset from a TEX/LATEX file prepared by the author.